Clays and Clay Minerals, Vol. 60, No. 3, 330–337, 2012.

EFFECTS OF Mg, Ca, AND Fe(II) DOPING ON THE KAOLINITE (001) SURFACE WITH H_2O ADSORPTION

MAN-CHAO HE AND JIAN ZHAO*

State Key Laboratory for Geomechanics and Deep Underground Engineering, China University of Mining and Technology, Beijing 100083, China

Abstract—Kaolinite is often a cause of deformation in soft-rock tunnel engineering, leading to safety problems. The mechanism of the deformation is closely related to the interaction between kaolinite and water molecules. Because kaolinite has multiple defects, the effects of Mg, Ca, and Fe(II) doping on the atomic structure of the kaolinite (001) surface, and the subsequent adsorption and penetration of H_2O into the interlayer, were studied systematically using density-functional theory. The results showed that for the Mg-, Ca-, and Fe(II)-doped kaolinites (001), the surface relaxation around the doping layer changed from contraction to expansion, due to the redistribution of electrons. The adsorption energies of the H_2O monomer on Mg-, Ca-, and Fe(II)-doped kaolinites (001) were less than on undoped kaolinite (001). The results further revealed that the H_2O molecule can also adsorb on the hollow site on the second-layer O surface of the Mg-, Ca-, and Fe(II)-doped kaolinites (001). For the undoped kaolinite, however, the H_2O molecule adsorbs on the surface only. The energetic barriers for penetration of H_2O from the adsorption site on the surface to the adsorption site on the O surface of Mg-, Ca-, and Fe(II)-doped kaolinites were also calculated: 1.18 eV, 1.07 eV, and 1.41 eV, respectively. The results imply that the influences of Mg, Ca, and Fe(II) doping on kaolinite allow the adsorbed water molecules to penetrate from the on-surface adsorption site to the O-surface site.

Key Words—Adsorption, First-principles Calculations, Kaolinite, Penetration, Point Defect.

INTRODUCTION

Soft rocks rich in clay minerals can cause harm to tunnel engineering because, when adsorbing water, the mechanical strength of the clay minerals is reduced, leading to deformation of the rocks. In order to gain a better predictive understanding of the governing principles associated with this phenomenon, the interaction between clay minerals and water molecules requires further investigation (Roland *et al.*, 2011; Croteau *et al.*, 2009). Kaolinite is one of the most abundant components in clay minerals and understanding the interaction between kaolinite and water molecules is important to researchers in the fields of geophysics and geomechanics (Yoshihiko *et al.*, 1999; He *et al.*, 2009; Gupta and Miller, 2010; Yin and Miller, 2012). Due to the limitations of experimental methods, theoretical analysis of the mechanism from a microscopic point of view will help to solve the engineering problems. Computer simulation based on the density-functional theory (DFT) has been proven to be a powerful and reliable tool to study water−solid interfaces at the molecular level (Yang *et al.*, 2004; Park and Sposito, 2004). The behavior of water at the kaolinite (001) surface using DFT has been investigated (Hu and Angelos, 2008). However, as indicated by Hinckley indexes ranging from 1.44 to 0.18 (Plançon *et al.*, 1997), natural kaolinite includes a large range of defect elements (Figure 1). The primary contaminant cations are Mg, Ca, and Fe(II) and the concentration ranges are 0.07−0.71 wt.%, 0.14−0.54 wt.%, and 0.07−0.31 wt.%, respectively (Chen and Wang, 2004; Frost *et al.*, 2004). The influences of Mg, Ca, and Fe(II) doping on the interaction between H_2O molecules and kaolinite have not yet been established (Jiang *et al.*, 2010; He *et al.*, 2000). Greater insight into the Mg, Ca, and Fe(II) doping effect of the interaction between water molecules and kaolinite (001), through detailed first-principles calculations, is needed.

The existing experimental (Adams, 1983; Benco *et al.*, 2001; Bish, 1993) and theoretical data (Hayashi, 1997; Hess and Saunders, 1992; Hobbs *et al.*, 1997; Plançon *et al.*, 1997; Teppen, *et al.*, 1997; Hu and Angelos, 2008) for the kaolinite $Al_2Si_2O_5(OH)_4$ surface are often rationalized by modeling two surfaces as almost perfect 1:1 layer structures consisting of two different surfaces of aluminosilicate. One side consists of a gibbsite-type sheet where Al ions are coordinated octahedrally by oxygen ions and hydroxyl groups; the other side of the layer consists of a silica sheet in which Si ions are coordinated tetrahedrally by only oxygen ions (Sato *et al.*, 2005). While the silica-sheet side is saturated and hydrophobic, the hydroxyl at the Al (oxyhydr)oxide side is hydrophilic. The (001) (basal) surface of kaolinite is that which is mainly exposed. In particular, the hydroxylated (001) surface is of primary interest in adsorption and penetration studies. Moreover,

* E-mail address of corresponding author:
zhaojian0209@yahoo.com.cn
DOI: 10.1346/CCMN.2012.0600309

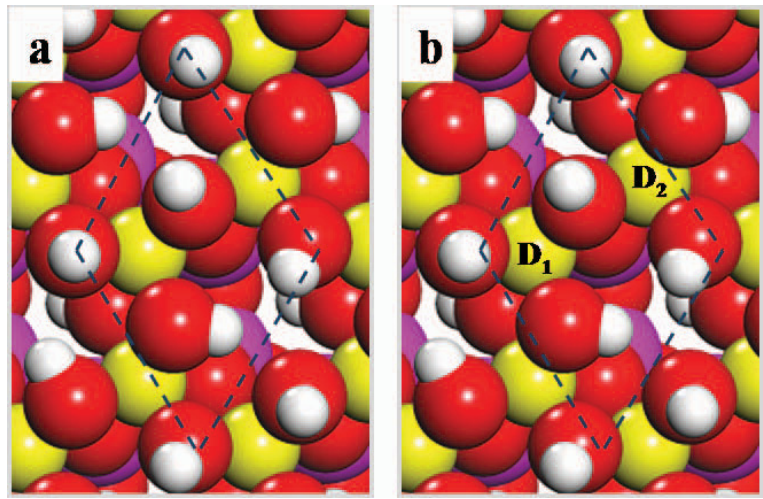

Figure 1. (a) Undoped kaolinite crystal structure seen from the hydroxylated (001) face. (b) Top view of two kinds of doping sites for defect-ion substitutions for Al in kaolinite (D_1 and D_2). Here, white spheres, red spheres, yellow spheres, and purple spheres represent H, O, Al, and Si, respectively.

because the void space between the second and third layers is large enough, the Al (001) face of the third layer is also of interest in adsorption studies such as the present one.

METHODS

The first-principles calculations were performed using the Vienna *ab inito* simulation package, *VASP* (Kresse and Furthmüller, 1996). Projector augmented-wave (PAW) pseudopotentials (Blöchl, 1994; Kresse and Joubert, 1999) were used. The energy cutoff for the plane waves was 400 eV. The undoped, Mg-doped, Ca-doped, and Fe(II)-doped kaolinite (001) surfaces were modeled by a slab made up of six atomic layers and a vacuum region of 20 Å, which was found to be sufficiently convergent. All the calculations were performed in a four-formula unit $Al_2Si_2O_5(OH)_4$ supercell with an Al ion replaced by a defect ion. The $2 \times 2 \times 1$ supercell was chosen to provide sufficient lattice sites to accommodate Mg, Ca, and Fe(II) concentrations as low as 1.47 mol.%. The H_2O molecule adsorbed and penetrated on one side of the slab. The Monkhorst–Pack scheme (Monkhorst and Pack, 1976) with $2 \times 2 \times 1$ k points was used to integrate in the irreducible bands around the Fermi energy (E_f) by a finite-T Fermi function and extrapolating to T = 0 K. During geometry optimizations, two layers at the bottom of the undoped and doped kaolinite (001) surfaces were fixed while other atoms were free to relax until the forces acting on them were <0.02 eV/Å. The calculated lattice parameters of bulk kaolinite were a = 5.160 Å, b = 5.160 Å, c = 7.602 Å, α = 81º, β = 89º, and γ = 60.18º, in good agreement with experimental lattice parameters reported previously (Hess and Saunders, 1992). The bond length and the H–O–H internal angle of a free H_2O molecule were calculated to be 0.97 Å and 104.6º, respectively.

RESULTS

The microscopic mechanisms of Mg, Ca, and Fe(II) ion doping in kaolinite were studied first before considering the effect of doping on the interaction between water molecules and kaolinite. The atomic structure for the relaxed kaolinite (001) surface was calculated (Figure 1a), during which the two kinds of high-symmetry doping sites (D_1 and D_2) for Mg, Ca, and Fe(II) to substitute for the Al ion in kaolinite were considered (Figure 1b). Following Wei and Zhang (2002), the defect formation energy $\Delta H_f(\alpha,q)$ as a function of the Fermi energy E_F and atomic chemical potential μ_i of the ith element were deduced. For the present system, $\Delta H_f(\alpha,q)$ is given by:

$$\Delta H_f(\alpha,q) = \Delta E(\alpha,q) + n_{Al}\mu_{Al} + n_{Si}\mu_{Si} + n_A\mu_A + n_O\mu_O + n_H\mu_H + qE_f \quad (1)$$

Here, $\Delta E(\alpha,q)$ can be determined by the following self-consistent total energy calculation:

$$\Delta E_f(\alpha,q) = \Delta E_f(\alpha,q) - E(\text{kaolinite}) + n_{Al}\mu^0_{Al} + n_{Si}\mu^0_{Si} + n_A\mu^0_A + n_O\mu^0_O + n_H\mu^0_H + qE_{VBM} \quad (2)$$

$E(\alpha,q)$ is the total energy of the supercell containing the defect α in charge state q, E(kaolinite) is the total energy of the defect-free supercell containing 68 atoms, and n_{Al}, n_{Si}, n_A, n_O, and n_H are the number of Al, Si, extrinsic defects (A), O, and H ions in the supercell, respectively. In the present case, the kaolinite kept its equilibrium with bulk Al, Si, and doped ions under ambient conditions and, therefore, μ^0_{Al}, μ^0_{Si}, and μ^0_A were identical to the ground-state energies (per ion) of bulk Al (cubic close-packed), Si (diamond structure), and doped

ions, *i.e.* $\mu^0_{Al} = E_{bulk}(Al)$, $\mu^0_{Si} = E_{bulk}(Si)$, and $\mu^0_A = E_{bulk}(A)$. Likewise, the chemical potentials μ^0_H and μ^0_O are given by half of the ground-state gas energies for hydrogen and oxygen molecules, respectively, *i.e.* $\mu^0_H = 0.5E_{H_2}$ and $\mu^0_O = 0.5E_{O_2}$. E_F in equation 1 is the Fermi energy measured from the valence band maximum (VBM), E_{VBM}. Depending on the experimental growth conditions, some thermodynamic limits exist for chemical potentials. In the present study, the chemical potential of kaolinite was not considered, *i.e.* all the results calculated were discussed for $\mu_i = 0$ in equation 1. The Mg, Ca, and Fe(II) defect-formation energies at D_1 doping sites were 3.25 eV, 3.31 eV, and −0.36 eV, respectively, and at D_2 doping sites they were 3.15 eV, 3.19 eV, and −0.58 eV, respectively. The results showed that Mg, Ca, and Fe(II) ions can easily substitute for Al ions. Interestingly, the Fe(II) ion has a negative formation energy, which means that the Fe(II) substitutes easily for the Al ion in kaolinite. The other defect ions, such as Mg and Ca as calculated above, require an observable amount of energy to substitute for the Al ion in kaolinite. Compared with the defect-formation energies at two doping sites, the results suggested that these three kinds of ions substitute more easily for the Al ion at the D_2 site.

The atomic structures for the relaxed kaolinite (001) surface (Figure 2), and of the Mg-, Ca-, and Fe(II)-doped kaolinite (001) surfaces were considered. During the geometry optimizations, the distances between the top-most four atomic layers of the undoped and doped kaolinite (001) were changed. To describe the changes more clearly, the surface relaxation is defined here as

$$\Delta d_{ij} = \frac{d_{ij} - d_0}{d_0} \quad (3)$$

where d_{ij} and d_0 are the distance between the ith and jth layer of the relaxed surface and the corresponding distance between the ith and jth layer of bulk kaolinite along the (001) direction, respectively. The calculated relaxations for the undoped and for the Mg-, Ca-, and Fe(II)-doped kaolinite (001) surfaces are summarized in Table 1. The distances between the top-most four atomic layers of the undoped kaolinite (001) surface contracted by 1.06, 0.04, and 0.02%, respectively. After Mg ion doping at the third layer, the distance between the first and second layer, d_{12}, decreased by 1.1%, but d_{23} and d_{34} expanded by 1.2 and 1.14%, respectively. Analogously, for the Ca-doped and Fe(II)-doped surfaces, d_{12} decreased by ~1.1 and 1.25%, respectively. The values for d_{23} and d_{34} expanded by ~1.2% for the Ca-doped and Fe(II)-doped surfaces. For the third layer, containing the doped Mg, Ca, and Fe(II) ions, the lattice spacing with respect to the nearest layer expanded considerably from that of bulk kaolinite.

One quantity tailored for the present study was the adsorption energy (E_{ads}) of the adsorbed H_2O molecule on Mg-, Ca-, or Fe(II)-doped kaolinite substrate, which is defined as:

$$E_{ads} = E_{H_2O} + E_{substrate} - E_{\frac{H_2O}{substrate}} \quad (4)$$

Here E_{H_2O}, $E_{substrate}$, and $E_{H_2O/substrate}$ are the total energies of the H_2O molecule, the doped kaolinite surface, and the total adsorption system, respectively. According to this definition, a positive value of E_{ads} indicated that the adsorption was exothermic (stable) and a negative value indicated endothermic (unstable) reaction. A single water molecule adsorbed on the surface and the void space between second and third layers of doped kaolinite (001) were investigated to give a general understanding of the water−kaolinite bonds. Four kinds of high-symmetry adsorption sites (Hu and Angelos, 2008) for H_2O were considered, including on-surface (three one-fold top sites T_1−T_3, three two-fold bridge sites B_1−B_3, and six three-fold hollow sites H_1−H_6) and Al-subsurface (one six-fold hollow site H_7) of the Mg-, Ca-, and Fe(II)-doped kaolinites (Masel, 1996), respectively (Figure 3). The O ion of water was initially placed on the precise high-symmetry sites with various orientations of water with respect to the substrate.

For optimization, the water molecule and doped kaolinite were allowed to relax fully and all of the initial structures with the water molecule adsorbed at the top and at the bridge sites moved to the three-fold hollow sites on the surface, which have proven to be the most stable sites for water-molecule adsorption on the surface (Hu and Angelos, 2008). In addition, upon optimization, the H_2O monomer was initially placed in the void space between the second and third layers relaxed to close the three-fold hollow site on the O-surface of the second layer of kaolinite. The adsorption energies of the water

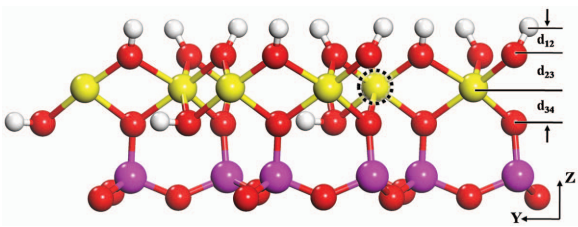

Figure 2. Atomic configurations of the kaolinite (001) surfaces. The yellow sphere marked with black dots represents the Al ion replaced by a defect.

Table 1. Surface relaxations (Δd_{12}, Δd_{23}, and Δd_{34}) of undoped and of Mg-, Ca-, and Fe(II)-doped kaolinites (001).

Surface	Δd_{12} (%)	Δd_{23} (%)	Δd_{34} (%)
Kaolinite (001)	−1.06	−0.04	−0.02
Mg-doped	−1.10	1.20	1.14
Ca-doped	−1.10	1.23	1.09
Fe(II)-doped	−1.25	1.46	1.37

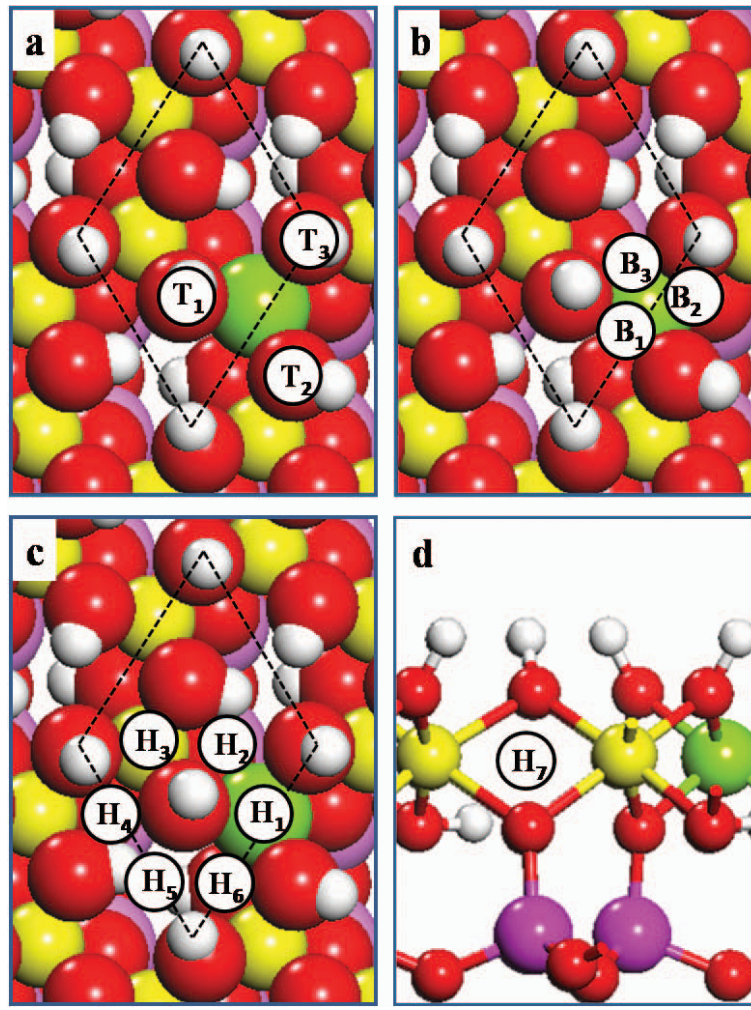

Figure 3. (a–c) Top view of defect-doped kaolinite (001) on the surface with three top adsorption sites (T_1–T_3), three bridge adsorption sites (B_1–B_3), and six three-fold hollow adsorption sites (H_1– H_6). (d) Side view of the void space of defect-doped kaolinite (001) with one six-fold adsorption site (H_7).

adsorbate on Mg-, Ca-, and Fe(II)-doped kaolinites were calculated (Table 2). The adsorption on three-fold hollow sites on the surface of Mg-, Ca-, and Fe(II)-doped kaolinites were preferred energetically within an observable energy which ranged from 0.95 to 1.1 eV/H_2O, 0.83 to 1.03 eV/H_2O, and 1.00 to 1.08 eV/H_2O, respectively. At these sites the H_2O monomer sat upright (Figure 4a). The most stable adsorption was found to be the three-fold hollow site H_5 of Mg-doped kaolinite. The O–H bond in H_2O was

Table 2. Calculated energies for monomer adsorption on six hollow adsorption sites on the surface and one hollow adsorption site on the Al surface of Mg-, Ca-, and Fe(II)-doped kaolinite (001). Adsorption energies, E_{ads} (in eV/H_2O), are listed. The first row lists the calculated values for adsorption of water molecules on the undoped kaolinite (001) surface for comparison.

E_{ads} (eV)	H_1	H_2	H_3	H_4	H_5	H_6	H_7
Undoped	1.07	1.06	1.10	1.06	1.15	1.07	–
Mg-doped	0.95	1.04	1.08	0.99	1.10	1.08	0.28
Ca-doped	0.83	0.96	0.85	0.90	1.03	0.90	0.26
Fe(II)-doped	1.01	1.07	1.02	1.03	1.08	1.00	0.20

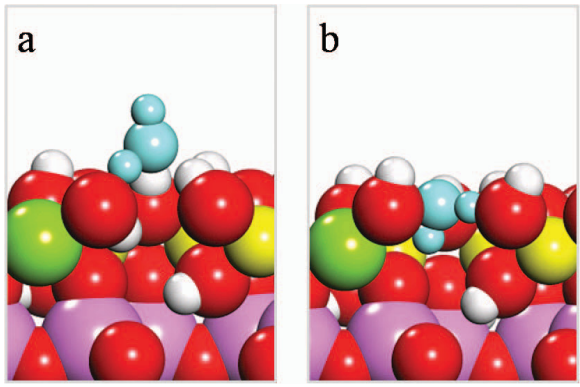

Figure 4. Side view of: an adsorbed water molecule on the surface of the hollow site (a); and the Al-surface hollow site (b) of defect-doped kaolinite.

elongated by 0.08 Å from a calculated gas phase value of 0.97 Å and the H−O−H internal angle was expanded by 5° from 104.6°.

In order to gain more insight into the precise nature of the chemisorbed molecular state, the electronic partial density of states (PDOS) of the H_2O molecule and of the top-most H layer were calculated. As a typical example, the PDOS for the most stable adsorption configuration of H_5 was plotted. For comparison, the PDOS of the free H_2O molecule and the top-most H layer of clean (*i.e.* kaolinite surface without H_2O adsorption) Mg-doped kaolinite (001) were also calculated (Figure 5). The three-dimensional (3D) electron density difference $\Delta\rho(r)$, which was obtained by subtracting the electron densities of non-interacting component systems, $\rho^{\text{kaolinite (001)}}(r) + \rho^{H_2O}(r)$, from the density $\rho(r)$ of the H_2O/kaolinite (001) surface, while retaining the atomic positions of the component system at the same location as in H_2O/kaolinite (001), is shown in the inset of Figure 5a. A positive (blue) $\rho(r)$ value indicated accumulation of electron density upon binding, while a negative (yellow) value corresponded to electron-density depletion. After adsorption, the 3σ, 4σ, and 5σ bonding molecular orbitals of H_2O shifted down in energy by 0.35, 0.75, and 0.34 eV, respectively. The results were essentially caused by the different electronegativities of kaolinite and water molecules which induce charge redistribution and, thus, build a global electrostatic attraction between the water and substrate. In addition, the amplitudes of 1π bonding and 2π anti-bonding orbitals were much weaker than those in free H_2O. Furthermore, the energy overlap between adsorbed H_2O and kaolinite (001) surface electrons ranged from −8.5 eV to the Fermi energy. All these features indicated a covalent coupling between the adsorbed water and the substrate; no charge transferred from the electronic states of kaolinite back to the H_2O molecule as no new orbital occupation in the PDOS of H_2O was seen after adsorption. This result was substantiated by the 3D electron-density difference. A large charge accumulation existed between the adsorbate and the substrate, and three hydrogen bonds were formed, among which one donates electrons from the water monomer to the substrate while two donate electrons from surface hydroxyl groups to the water monomer.

The hollow site H_7 was proven to be the only stable adsorption site for the H_2O monomer on the O surface of Mg-, Ca-, and Fe(II)-doped kaolinites. The adsorption energies for H_7 of Mg-, Ca-, and Fe(II)-doped kaolinites

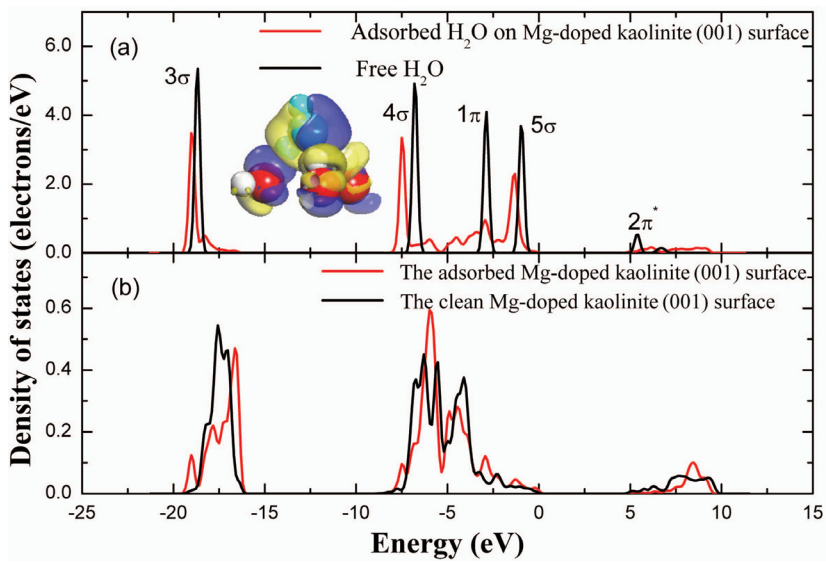

Figure 5. Electronic partial density of states plots for the H_2O molecule and the top-layer H ions bonded to H_2O at the stable three-fold hollow adsorption site on the surface: (a) free and adsorbed H_2O molecule, where the inset shows the side view of electron density difference for a water molecule at the stable adsorption site; and (b) clean and adsorbed kaolinite (001) surface. The Fermi energy is set at zero.

were 0.28, 0.26, and 0.20 eV less than the on-surface adsorption sites, respectively. Compared with Ca-doped and Fe(II)-doped kaolinites, the adsorption site H_7 of Mg-doped kaolinite had the largest adsorption energy. As a typical example, the O–H bond in H_2O was elongated to 1.09 Å from a calculated gas-phase value of 0.97 Å and the H–O–H internal angle was expanded by 0.6° from 104.6°. In the plane of the O-surface normal, one O–H bond of H_2O pointed to an oxygen ion as a proton donor and two hydroxyls of the surface pointed to the oxygen ion of the H_2O molecule. The other H ion of H_2O pointed to an oxygen ion of the fourth O layer (Figure 4b). In order to further understand the precise nature of the chemisorbed molecular state, the electronic PDOS of the H_2O molecule and the second O layer were plotted (Figure 6). The difference between the three-dimensional (3D) electron density $\Delta\rho(r)$ and the density $\rho(r)$ of the H_2O/Mg-doped kaolinite (001) surface is shown in the inset of Figure 6a. After adsorption, the 3σ and 4σ bonding molecular orbitals of H_2O shifted down in energy by 1.5 and 1.37 eV, respectively, while the 5σ shifted up by 1.06 eV. In addition, the amplitudes of all bonding orbitals were much weaker than those in free H_2O. These features were essentially caused by the different electronegativities of the kaolinite and water molecules, which induced charge redistribution and, thus, built a global electrostatic attraction between the water and the O substrate. Furthermore, the s and p electronic states of the adsorbed kaolinite (001) O surface expanded in energy compared with the clean kaolinite (Figure 6b,c). For Mg-doped surface states, new peaks appeared, aligning in energy with the 3σ, 4σ, and 5σ bonding orbitals of H_2O, indicating a weak hybridization contribution to the molecule–solid interaction. The results were substantiated by the 3D electron density difference. Between the adsorbate and substrate a large charge accumulation existed. To compare, the adsorption of the H_2O monomer on the same void space between the second and third layers of undoped kaolinite was calculated. The results revealed that the H_2O monomer cannot adsorb on the void space of undoped kaolinite (001). In fact, after relaxation, the water molecule initially placed in the void space will segregate spontaneously onto the surface without encountering an energy barrier.

Because the most favorable adsorption sites on the outer surface and at the O-surface were the three-fold hollow H_5 and H_7 sites, respectively, no geometric obstacle existed between H_5 and H_7, leading to speculation that, at low temperature, the H_2O on surface hollow sites may penetrate to the O-surface hollow sites by overcoming a relatively low barrier. The penetration energy path from the H_2O of on-surface H_5 to the O-surface H_7 in the Mg-, Ca-, and Fe(II)-doped kaolinites using the nudged elastic band method (Roehl *et al.*, 2010) were investigated. The difference between the

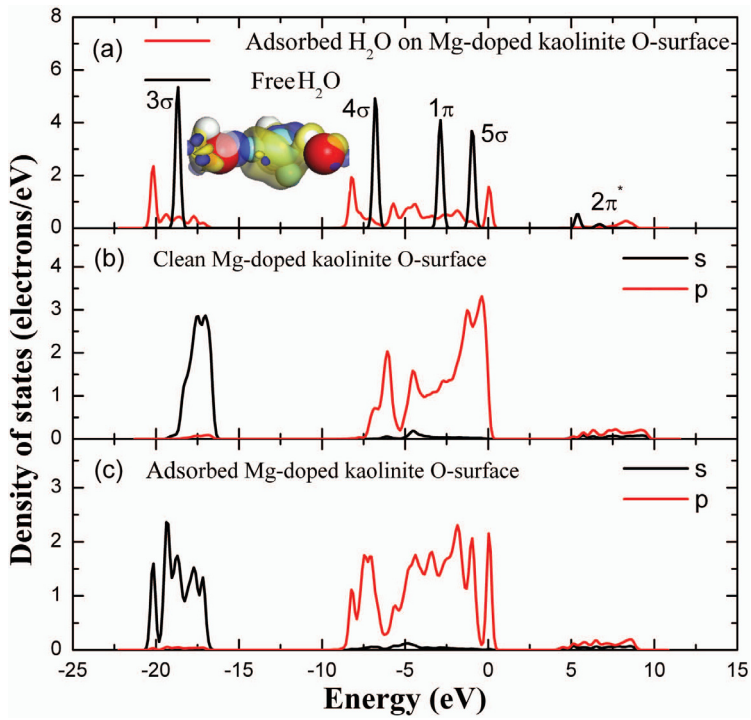

Figure 6. Electronic partial density of states plots for the H_2O molecule and the second-layer O ions bonded to H_2O at the stable hollow adsorption site on the subsurface: (a) free and adsorbed H_2O molecule, where the inset shows the electron density difference for the water molecule at the stable adsorption site; (b–c) clean and adsorbed kaolinite (001) O-surface. The Fermi energy is set at zero.

highest energy and that of the initial binding site was taken as the penetration barrier (Michaelides *et al.*, 2004). The penetration path between hollow H_5 on-surface and hollow H_7 O-surface sites was modeled using nine images. The route was investigated by moving H_2O from the initial to the final hollow site and seven linear interpolations between the initial and final positions. Given a H_2O monomer at the hollow site H_5 on-surface, movement through the (001) surface to the hollow site H_7 at the O surface was then investigated.

The activation energies, E_a, determined from the three penetration energy paths, were investigated. The E_a for a given route was the energy difference between the highest and lowest energy points along that route. The activation energies for the Mg-, Ca-, and Fe(II)-doping routes were calculated to be 1.18, 1.07, and 1.41 eV, respectively (Figure 7). The three penetration paths encountered two small, different activation barriers. For H_2O to penetrate from one hollow site on the surface to another hollow site at the O surface, a relatively small energy barrier must be overcome. The transition state, *i.e.* the atomic geometry of the energy maximum in the penetration path, corresponded to the atoms of the H_2O monomer at the surface H layer. When the H_2O monomer penetrated from H_5 to H_7, the distance of the O ion from the top-most H layer changed from 0.9 to −0.7 Å, 0.9 to −0.5 Å, and 0.9 to −1.1 Å, respectively.

SUMMARY

The effects of the doping of Mg, Ca, and Fe(II) ions in the atomic structure of the kaolinite (001) surface and the adsorption and penetration behaviors of the H_2O molecule were examined using the plane-wave pseudopotential formalism of DFT. The results showed that doping with Ca, Mg, or Fe(II) changed the surface atomic structure. Due to redistribution of electrons, the surface relaxation changed from contraction to expansion around the doping layer. The results showed that H_2O adsorbs preferentially on the surface three-fold hollow sites of Mg-, Ca-, and Fe(II)-doped kaolinites (001) with the adsorption energies ranging from 0.95 to 1.1 eV/H_2O, 0.83 to 1.03 eV/H_2O, and 1.00 to 1.08 eV/H_2O, respectively, which are less than undoped kaolinite. At the hollow sites, the H_2O molecule formed three hydrogen bonds with the surface hydroxyl groups.

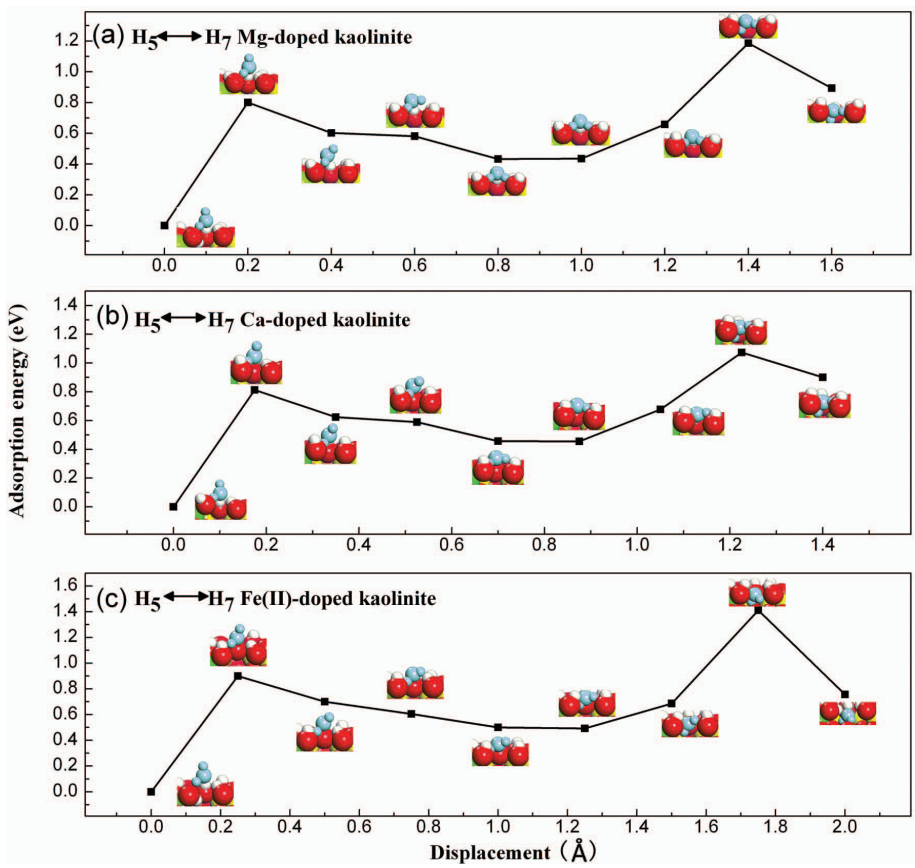

Figure 7. Variation in H_2O adsorption energy from the original three-fold hollow site for the H_2O penetration route on kaolinite (001). The structure of the initial, transition, and final states of the pathway are also shown. The solid lines connecting the data points are guides to the eye.

From PDOS and electron density difference analysis, the hollow site on the O surface also proved to be the only stable adsorption site for chemisorbed H_2O of Mg-, Ca-, and Fe(II)-doped kaolinites. However, the H_2O molecule cannot adsorb on the undoped kaolinite O surface. Finally, the energetic barriers for penetration of H_2O from the adsorption site on the surface to an adsorption site on the O surface of Mg-, Ca-, and Fe(II)-doped kaolinites, which were 1.18, 1.07, and 1.41 eV, respectively, implied that the effects of Mg, Ca, and Fe(II) doping make it easier for water molecules to penetrate from the on-surface site to the O-surface site. The simulations above show the key role played by defects during the interaction between water and kaolinite, which explains the deformation problem for soft rocks, *i.e*. the reduction in mechanical strength and the increase in structural deformation of soft rock upon adsorption of water.

ACKNOWLEDGMENTS

The research above was supported by the Program for Changjiang Scholars and Innovative Research Team at the University of China under Grant No. IRT0656, and the National Natural Science Foundation of China (No 40972196 and 41172263)

REFERENCES

Adams, J.M. (1983) Hydrogen ion position in kaolinite by neutron profile refinement. *Clays and Clay Minerals*, **31**, 352–358.

Benco, L., Tunega, D., Hafner, J., and Lischka, H. (2001) Orientation of OH groups in kaolinite and dickite: *ab initio* molecular dynamics study. *American Mineralogist*, **86**, 1057–1065.

Bish, D.L. (1993) Rietveld refinement of the kaolinite structure at 1.5 K. *Clays and Clay Minerals*, **41**, 738–744.

Blöchl, P.E. (1994) Projector augmented-wave method. *Physical Review B*, **50**, 17953–17979.

Chen, J. and Wang, H.N. (2004) Pp. 35–60 in: *Geochemistry* (H.Y. Xie and P. Liu,editors). Science Press, Beijing.

Croteau, T., Bertram, A.K., and Patey, G.N. (2009) Simulation of water adsorption on kaolinite under atmospheric conditions. *The Journal of Physical Chemistry A*, **113**, 7826–7833.

Frost, R.L., Horváth, E., Makó, E., and Kristóf, J. (2004) Modification of low- and high-defect kaolinite surfaces: implications for kaolinite mineral processing. *Journal of Colloid and Interface Science*, **270**, 337–346.

Gupta, V. and Miller, J.D. (2010) Surface force measurements at the basal planes of ordered kaolinite particles. *Journal of Colloid and Interface Science*, **344**, 362–371.

Hayashi, S. (1997) NMR study of dynamics and evolution of guest molecules in kaolinite/dimethyl sulfoxide intercalation compound. *Clays and Clay Minerals*, **45**, 724–732.

He, M.C., Jing, H.H., and Yao, A.J. (2000) Research progress of soft rock engineering geomechanics in China coal mine. *Journal of Engineering Geology*, **1**, 46–62.

He, M.C., Fang, Z.J., and Zhang, P. (2009) Theoretical studies on the defects of kaolinite in clays. *Chinese Physics Letters*, **26**, 059101–059104.

Hess, A.C. and Saunders, V.R. (1992) Periodic ab initio Hartree-Fock calculation of the low-symmetry mineral kaolinite. *The Journal of Physical Chemistry*, **11**, 4367–4374.

Hobbs, J.D., Cygan, R.T., Nagy, K.L., Schultz, P.A., and Sears, M.P. (1997) All-atom *ab initio* energy minimization of the kaolinite crystal structure. *American Mineralogist*, **82**, 657–662.

Hu, X.L. and Angelos, M. (2008) Water on the hydroxylated (001) surface of kaolinite: from monomer adsorption to a flat 2D wetting layer. *Surface Science*, **602**, 960–974.

Jiang, M.Q., Jin, X.Y, Lu, X.Q., and Chen, Z.L. (2010) Adsorption of Pb(II), Cd(II), Ni(II), and Cu(II) onto natural kaolinite clay. *Desalination*, **252**, 33–39.

Kresse, G. and Furthmuller, J. (1996) Efficient iterative schemes for ab initio total-energy calculations using a plane-wave basis set. *Physical Review B*, **54**, 11,169–11,173.

Kresse, G. and Joubert, J. (1999) From ultrasoft pseudopotentials to the projector augmented-wave method. *Physical Review B*, **59**, 1758–1762.

Masel, R.L. (1996) *Principles of Adsorption and Reaction on Solid Surfaces.* Wiley, New York, pp. 22–24.

Michaelides, A., Ranea, V.A., de Andres, P.L., and King, D.A. (2004) First-principles study of H_2O diffusion on a metal surface: H_2O on Al{100}. *Physical Review B*, **69**, 075409–075413.

Monkhorst, H.J. and Pack, J.D. (1976) Special points for Brillouin-zone integrations. *Physical Review B*, **13**, 5188–5192.

Park, S.H. and Sposito, G. (2004) Molecular modeling of clay mineral structure and surface chemistry. Pp. 39–90 in: *Handbook of Layered Materials* (P.K. Dutta, S.M. Auerbach, and K.A. Carrado, editors). CRC Press, Boca Raton, Florida, USA.

Plançon, A., Giese, R.F. Jr., Snyder, R., Drits, V.A., and Bookin, A.S. (1997) Stacking faults in the kaolinite-group minerals: defect structures of kaolinite. *Clays and Clay Minerals*, **37**, 195–198.

Roehl, J.L., Kolagatla, A., Ganguri, V.K.K., Khare, S.V., and Phaneuf, R.J. (2010) Binding sites and diffusion barriers of a Ga adatom on the GaAs(001)-c(4 × 4) surface from first-principles computations. *Physical Review B*, **82**, 165335–165340.

Roland, S., Martin, H.G., Hans, L., and Daniel, T. (2011) Wettability of kaolinite (001) surfaces – molecular dynamic study. *Geoderma*, **169**, 47–54.

Sato, H., Ono, K., Johnston, C.T., and Yamagishi, A. (2005) First-principles studies on the elastic constants of a 1:1 layered kaolinite mineral. *American Mineralogist*, **90**, 1824–1826.

Teppen, B.J., Rasmussen, K., Bertsch, P.M., Miller, D.M., and Schäferll, L. (1997) Molecular dynamic modeling of clay minerals. 1. Gibbsite, kaolinite, pyrophyllite, and beidellite. *The Journal of Physical Chemistry B*, **101**, 1579–1587.

Yang, J.Y., Meng, S., Xu, L.F., and Wang, E.G. (2004) Ice tessellation on a hydroxylated silica surface. *Physical Review Letters*, **92**, 146,102–146,105.

Yin, X. and Miller, J.D. (2012) Wettability of kaolinite basal planes based on surface force measurements using atomic force microscopy. *Minerals & Metallurgical Processing* (Special Industrial Minerals Issue), **29**, 13–19.

Yoshihiko, K., Yoshiyuki, S., and Kazuyuki, K. (1999) Intercalation of alkylamines and water into kaolinite with methanol kaolinite as an intermediate. *Applied Clay Science*, **15**, 241–252.

Wei, S.H. and Zhang, S.B. (2002) Chemical trends of defect formation and doping limit in II-VI semiconductors: The case of CdTe. *Physical Review B*, **66**, 155211–155221.

(*Received 18 January 2012; revised 13 June 2012; Ms. 638; AE: R.J. Pruett*)